JPE 16-2-27

http://dx.doi.org/10.6113/JPE.2016.16.2.675
ISSN(Print): 1598-2092 / ISSN(Online): 2093-4718

Sliding Mode Control of a New Wind-Based Isolated Three-Phase Induction Generator System with Constant Frequency and Adjustable Output Voltage

Mohammadreza Moradian† and Jafar Soltani*

†Department of Electrical Engineering, Science and Research Branch, Islamic Azad University, Tehran, Iran
* Department of Electrical Engineering, Khomeinishahr Branch, Islamic Azad University, Isfahan, Iran

Abstract

This paper presents a new stand-alone wind-based induction generator system with constant frequency and adjustable output voltage. The proposed generator consists of a six-phase cage-rotor induction machine with two separate three-phase balanced stator windings and a three-phase space vector pulse width modulation inverter that operates as a static synchronous compensator (STATCOM). The first stator winding is fed by the STATCOM and used to excite the machine while the second stator winding is connected to the generator external load. The main frequency of the STATCOM is determined to be constant and equal to the load-requested frequency. The generator output frequency is independent of the load power demand and its prime mover speed because the frequency of the induced emf in the second stator winding is the same as this constant frequency. A sliding mode control (SMC) is developed to regulate the generator output voltage. A second SMC is used to force the zero active power exchanged between the machine and the STATCOM. Some simulation and experimental results are presented to prove the validity and effectiveness of the proposed generator system.

Key words: Cage-rotor induction generator, Sliding mode control, Space vector pulse width modulation, Static VAR compensator, Wind power generation

I. INTRODUCTION

Rotating electrical energy conversion systems, which are driven by wind turbines, have been widely used all over the world. Similarly, wind energy conversion systems are suitable for isolated and remote areas [1] and are known to employ either synchronous or induction machines as their generator systems. Compared with synchronous machines, cage-rotor induction machines (CRIMs) feature low cost, simple construction, and little maintenance. Moreover, CRIMs are considerably reliable and rugged [2], [3].

Self-excited induction generators (SEIGs) are usually used to feed autonomous loads. However, SEIGs suffer from poor voltage and frequency regulation characteristics [4]-[7]. In other words, generator output voltage and frequency change under the influence of load power demand or rotor speed variations. Furthermore, the magnetizing reactive power of SEIGs must be supplied by an appropriate source [8], [9]. Using a full-rate back-to-back (BTB) converter is a direct method to solve these problems. Such BTB converters impose additional cost upon the system, especially in high-power ratings.

The popular wound-rotor doubly fed induction generator (DFIG) system needs to use a fraction-rate multi-quadrant BTB converter in the rotor circuit [10]. Unlike SEIGs, DFIG systems are highly expensive and require a complicated control scheme. However, the output frequency of a DFIG system is constant and independent of load power demand and prime mover speed.

The three-phase permanent magnet synchronous generator (PMSG) with a full-rate BTB converter is an attractive type of wind-based generation system. Although PMSGs have high power density and efficiency, they are susceptible to permanent magnet demagnetization and startup difficulties because of their cogging torque [11].

Manuscript received Jul. 4, 2015; accepted Oct. 31, 2015
Recommended for publication by Associate Editor Dong-Myung Lee.
†Corresponding Author: m.moradian@srbiau.ac.ir
Tel: +98-314-229-2623, Fax: +98-314-229-1016, Islamic Azad Univ.
*Dept. of Electrical Eng., Khomeinishahr Branch, Islamic Azad University, Iran

Today, multi-phase machines are used in wind turbine generation systems because of their desirable properties, such as low per-phase power rating requirement, minor torque ripple, and good fault tolerances [12]. Six-phase SEIGs were respectively modeled, implemented, and analyzed in [1], [2], and [12]-[14]. One of the best configurations in the proposed multi-phase generators is the brushless DFIG. Although brushless DFIGs enjoy the advantage of low-cost converters and do not require brush gears, they are not highly attractive because they require specially designed machines. In brushless DFIGs, the pole numbers of two stator windings are chosen so as to avoid direct coupling, and a special rotor design is needed to couple with the two stator windings. The nested loop type is the most widely used rotor [15]. In [16]-[18], a double winding induction generator (IG) was used to generate a variable-frequency ac power. The proposed generation systems in [16]-[18] are only applicable to special loads, such as the main demand of some giant civil airplanes in which frequency variations are not important (A380 and B787).

Although the abovementioned generation systems are widely used in wind energy conversion systems, there is a need for a CRIM-based system which its output frequency is intrinsically constant and independent of the prime mover speed and load power demand. Such system should be capable of delivering converted energy to the local load or main grid without a BTB converter so as to significantly reduce the overall system cost.

A single-phase IG with a constant frequency independent of prime mover speed and generator load demand was described in [19]. This generator is excited by a single-phase pulse width modulation (PWM) inverter, which feeds the stator auxiliary winding of the machine. The main stator winding is connected to a single-phase load. In the continuation of the research work described in [19], a single-phase IG was proposed with a three-phase CRIM [20]. The first stator reference phase of the machine is fed by a single-phase static synchronous compensator (STATCOM) and is used to excite the machine while the series connection of the other two phases is connected to a single-phase load. The authors of [20] proposed a three-phase double stator winding IG in [21]. The first three-phase stator winding is fed by a three-phase PWM voltage source inverter and is used to excite the machine. The second stator winding is connected to a three-phase balanced load. In this three-phase generator, similar to the single-phase IGs described in [19] and [20], the generator output frequency is constant and independent of the generator active power demand and its prime mover speed. The generator system described in [21] is driven by a hydro-turbine and is supported only by computer simulation results.

The research work described in this paper is in fact a continuation of the previous work described in [21]. Specifically, the research is conducted for the following purposes:

1- Adjustment of the rotor speed to force the STATCOM to only inject the reactive power into the IG and its local load
2- Usage of sliding mode controllers (SMCs) instead of conventional PI controllers to improve the system robustness against the system parameter uncertainties and load disturbances
3- Improvement and extension of the system modeling equations based on space vectors for an arbitrary space angle phase α difference between stator winding sets
4- Practical implementation of the proposed generator system by assuming a three-phase balanced load and a dc motor as its prime mover
5- Modeling of an adjustable speed wind turbine as the prime mover of the generator system

In this work, we introduce a stand-alone three-phase induction generator system (IGS), which consists of a six-phase CRIM with two sets of balanced stator windings and a three-phase space vector- (SV-) PWM inverter that operates as a STATCOM. In this generator scheme, one of the stator windings, hereafter called excitation winding (EW), is fed by a three-phase STATCOM. At the same time, the second stator winding, hereafter called power winding (PW), is connected to a three-phase local load. The main frequency of the STATCOM is chosen to be exactly equal to the load desired frequency. Since the machine air-gap magnetic flux vector rotates at this frequency, therefore the frequency of the induced emf in the PW is the same as this constant frequency. Under generator loading conditions, the generator output frequency remains constant and independent of the load power demand and generator prime mover speed. An adjustable speed wind or a hydro-turbine can be used as a generator prime mover. An SMC is designed to regulate the generator output voltage, and a second SMC is developed to force the EW to only feed the reactive power to the machine. To regulate the generator output voltages, the first SMC generates STATCOM reference voltages. The frequency of these STATCOM reference voltages is chosen to be equal to the desired generator output frequency. For a given three-phase load, the second SMC produces the rotor reference speed such that no active power exchange occurs between the machine and the STATCOM. The proposed IGS is practically implemented using a dc motor as the main prime mover of the system. The simulation results are obtained with an adjustable-speed wind turbine based on a pitch angle controller. Some simulation and experimental results confirm the validity and effectiveness of the performance of the proposed IGS.

The advantages of the IGS proposed in this work, in comparison with isolated systems based on DFIGs or PMSGs/SEIGs with a full-rate BTB converter, are summarized as follows.

- As the generator output frequency is constant and independent of the load power demand and generator prime mover speed, the proposed IGS can directly feed local loads even without BTB converters and droop-based

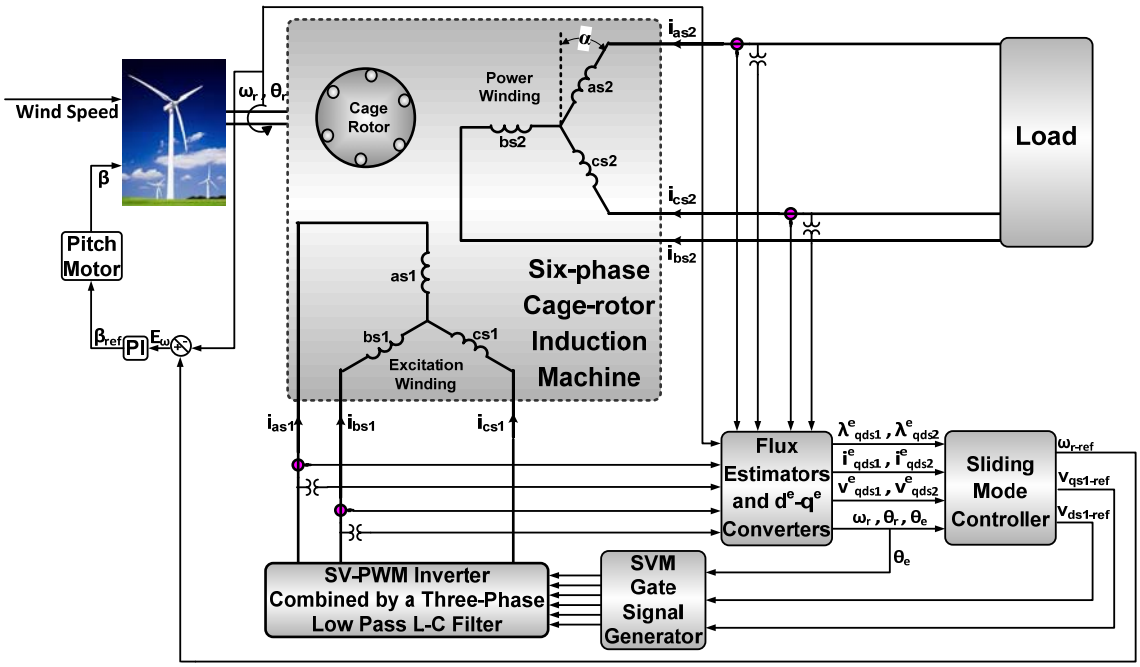

Fig. 1. Overall system configuration.

controllers.

- Assuming similar power, voltage, and current ratings, the price of the PMSG or wound-rotor induction machine is extremely higher than that of a CRIM. In addition, CRIMs feature a simpler and more rugged construction, greater reliability, and less maintenance requirements compared with wound-rotor induction machines or PMSGs. In addition, PMSGs are susceptible to permanent magnet demagnetization and startup difficulties because of cogging torque.
- The proposed IGS only requires a fraction-rate STATCOM to excite the machine instead of a multi-quadrant BTB converter.
- As the two sets of stator windings are not physically connected and are only electromagnetically linked, the influence of inverter-induced harmonics on generator load voltages and currents is minimal.
- The closed-loop control system of the proposed IGS is simpler and more practical than that of PMSGs/SEIGs or DFIGs.

II. IGS Mathematical Model

The overall configuration of the proposed IGS is shown in Fig. 1. The IGS modeling based on the figure is described below.

A. Machine Model

In a three-phase ac machine, the space vector of a general variable f_i in the stationary reference frame is defined by [22]

$$\bar{f}_i^s = \frac{2}{3}(f_{ai} + \mathrm{a} f_{bi} + \mathrm{a}^2 f_{ci}) = f_{di}^s + j f_{qi}^s \tag{1}$$

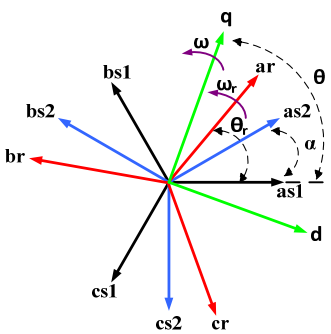

Fig. 2. Phasor diagram of the generator.

where f_i denotes the voltage, current, and linkage flux; superscript s denotes the stationary reference frame; and subscript i stands for either stator ($i = s$) or rotor ($i = r$) variables. According to [22], the space vector $\bar{f}_i^s$ in the synchronous reference frame is defined by

$$\bar{f}_i^e = f_{di}^e + j f_{qi}^e = \bar{f}_i^s e^{-j\omega_e t} \tag{2}$$

where superscript e denotes the synchronous reference frame and ω_e indicates the synchronous electrical angular speed of the machine.

The phasor diagram of the generator windings is illustrated in Fig. 2. Two three-phase stator windings are located in α electrical degree spatial phase difference related to each other.

The equivalent generator windings in the (d^e, q^e) synchronous reference frame are shown in Fig. 3.

Referring to [22], the induction machine voltage space vectors in the (d^e, q^e) synchronous reference frame are

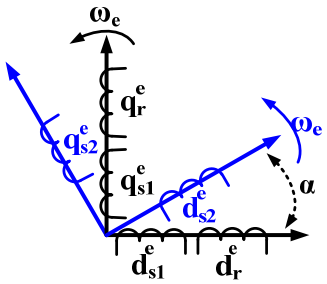

Fig. 3. Representation of generator windings in the (d^e, q^e) reference frame.

described by

$$\bar{v}_{s1}^{e} = \dot{\bar{\lambda}}_{s1}^{e} + R_{s1}\bar{i}_{s1}^{e} + j\,\omega_e\bar{\lambda}_{s1}^{e} \tag{3}$$

$$\bar{v}_{s2}^{e} = \dot{\bar{\lambda}}_{s2}^{e} + R_{s2}\bar{i}_{s2}^{e} + j\,\omega_e\bar{\lambda}_{s2}^{e} \tag{4}$$

$$\bar{v}_{r}^{e} = \dot{\bar{\lambda}}_{r}^{e} + R_{r}\bar{i}_{r}^{e} + j\,(\omega_e - \omega_r)\bar{\lambda}_{r}^{e} \tag{5}$$

where subscripts *s1, s2,* and *r* refer to EW, PW, and rotor variables, respectively; ω_r is the rotor electrical angular speed; $\bar{v}_{s1}^{e}, \bar{v}_{s2}^{e}, \bar{v}_{r}^{e}$ are the machine voltage space vectors; $\bar{\lambda}_{s1}^{e}, \bar{\lambda}_{s2}^{e}, \bar{\lambda}_{r}^{e}$ are the space vectors of the machine linkage fluxes; $\bar{i}_{s1}^{e}, \bar{i}_{s2}^{e}, \bar{i}_{r}^{e}$ are the machine current space vectors; and R_{s1}, R_{s2}, R_r are the stator and rotor winding resistances.

The space vectors of the machine linkage fluxes in the (d^e, q^e) synchronous reference frame are described as

$$\bar{\lambda}_{s1}^{e} = L_{s1}\bar{i}_{s1}^{e} + L_m\bar{i}_{s2}^{e}e^{j\alpha} + L_m\bar{i}_{r}^{e} \tag{6}$$

$$\bar{\lambda}_{s2}^{e} = L_m\bar{i}_{s1}^{e}e^{-j\alpha} + L_{s2}\bar{i}_{s2}^{e} + L_m\bar{i}_{r}^{e}e^{-j\alpha} \tag{7}$$

$$\bar{\lambda}_{r}^{e} = L_m\bar{i}_{s1}^{e} + L_m\bar{i}_{s2}^{e}e^{j\alpha} + L_r\bar{i}_{r}^{e} \tag{8}$$

with

$$\begin{aligned} L_{s1} &= L_{ls1} + L_m \\ L_{s2} &= L_{ls2} + L_m \\ L_r &= L_{lr} + L_m \end{aligned} \tag{9}$$

where L_m is the spatial magnetizing inductance; L_{ls1}, L_{ls2}, L_{lr} are the leakage inductances of machine windings; and L_{s1}, L_{s2}, L_r are the spatial machine self-inductances.

A static *(R, L)* three-phase balanced load is assumed to be supplied by the generator. In this case, the load equation in the (d^e, q^e) reference frame is described by

$$\bar{v}_{s2}^{e} = -R\,\bar{i}_{s2}^{e} - L\dot{\bar{i}}_{s2}^{e} - jL\omega_e\,\bar{i}_{s2}^{e} \tag{10}$$

The machine mechanical equation is

$$J\dot{\omega}_m = T_{turb} - T_e - B\,\omega_m \tag{11}$$

with

$$T_e = \frac{3}{2}(\lambda_{ds2}^{e}i_{qs2}^{e} - \lambda_{qs2}^{e}i_{ds2}^{e}) \tag{12}$$

where T_e is the generator electromagnetic torque, T_{turb} is the generator prime mover torque, ω_m is the rotor mechanical angular speed, J is the rotor moment of inertia, and B is the friction coefficient.

B. Generator State Space Model

The machine state space equation in matrix form is

$$\dot{\mathbf{X}} = \mathbf{F}(\mathbf{X}) + \mathbf{G}(\mathbf{X})\mathbf{U} \tag{13}$$

with

$$\mathbf{X} = [i_{qs1}^{e}\ \ i_{ds1}^{e}\ \ \lambda_{qs1}^{e}\ \ \lambda_{ds1}^{e}\ \ i_{qs2}^{e}\ \ i_{ds2}^{e}\ \ \omega_r]^T \tag{14}$$

$$\mathbf{U} = \begin{bmatrix} v_{qs1}^{e} & v_{ds1}^{e} & T_{turb} \end{bmatrix}^T \tag{15}$$

$$\mathbf{F}(\mathbf{X}) = [f_1\ \ f_2\ \ f_3\ \ f_4\ \ f_5\ \ f_6\ \ f_7]^T \tag{16}$$

$$\mathbf{G} = \begin{bmatrix} a_{11} & 0 & 1 & 0 & a_{21} & -a_{22} & 0 \\ 0 & a_{11} & 0 & 1 & a_{22} & a_{21} & 0 \\ 0 & 0 & 0 & 0 & 0 & 0 & 1/J \end{bmatrix}^T \tag{17}$$

The f_i functions and a_{ij} coefficients are given in Appendix A.

C. Wind Turbine Model

The mechanical power developed by a wind turbine is given by [23]

$$P_w = \frac{1}{2}\rho\pi r^2 C_p(\lambda,\beta)V_{wind}^3 \tag{18}$$

where P_w is the turbine mechanical output power, ρ is the air density, r is the radius of the turbine blades, V_{wind} is the wind speed, $C_P(\lambda, \beta)$ is the power coefficient of the wind turbine, β is the pitch angle of the turbine blades, and λ is the tip speed ratio, which is defined as:

$$\lambda = \frac{r\,\omega_{rt}}{V_{wind}} \tag{19}$$

where ω_{rt} is the angular speed of the turbine shaft. Referring to [24], the power coefficient of a wind turbine is given as

$$C_p = (0.44 - 0.0167\beta)\sin\left(\frac{\pi(\lambda-3)}{15-0.3\beta}\right) - 0.00184\beta(\lambda-3) \tag{20}$$

III. Sliding Mode Controllers

A first SMC is designed for the proposed IGS output voltage regulation and a second SMC is developed to regulate the exchanging active power between the EW and the STATCOM equal to zero.

The first SMC is designed to regulate the generator output voltage in the following way:

$$\mathbf{Y_{12}} = \begin{bmatrix} y_1 & y_2 \end{bmatrix}^T = \begin{bmatrix} v_{qs2}^{e} & v_{ds2}^{e} \end{bmatrix}^T \tag{21}$$

$$\mathbf{U_{12}} = \begin{bmatrix} u_1 & u_2 \end{bmatrix}^T = \begin{bmatrix} v_{qs1-ref}^{e} & v_{ds1-ref}^{e} \end{bmatrix}^T \tag{22}$$

The output voltage error signals are defined as

$$\begin{cases} e_{vqs2} = v_{qs2}^{e} - v_{qs2-ref}^{e} \\ e_{vds2} = v_{ds2}^{e} - v_{ds2-ref}^{e} \end{cases} \tag{23}$$

where $v_{qs2-ref}^{e}$ and $v_{ds2-ref}^{e}$ are the voltage references of the generator load. By substituting Equ. (4) with Equ. (7) and rewriting it in terms of the state variables, the following

equations can be obtained:

$$\begin{bmatrix} v_{qs2}^{e} \\ v_{ds2}^{e} \end{bmatrix} = \begin{bmatrix} z_1 & z_2 \\ -z_2 & z_1 \end{bmatrix} \begin{bmatrix} v_{qs1}^{e} \\ v_{ds1}^{e} \end{bmatrix} + \begin{bmatrix} E_1(\mathbf{X}) \\ E_2(\mathbf{X}) \end{bmatrix} \tag{24}$$

The z_i coefficients and E_i functions are defined in Appendix B. The following sliding mode switching surfaces are chosen:

$$\mathbf{S_{12}} = \begin{bmatrix} S_1 \\ S_2 \end{bmatrix} = \begin{bmatrix} e_{vqs2} + k_{1v} \int e_{vqs2}\, dt \\ e_{vds2} + k_{2v} \int e_{vds2}\, dt \end{bmatrix} \tag{25}$$

where K_{1v} and K_{2v} are constant positive coefficients.

Referring to [25], when the system states reach the sliding manifold and slide along the surface,

$$\mathbf{S_{12}} = \dot{\mathbf{S}}_{\mathbf{12}} = 0 \tag{26}$$

Combining Equs. (23)–(25) results in

$$\dot{\mathbf{S}}_{\mathbf{12}} = \begin{bmatrix} \dot{S}_1 \\ \dot{S}_2 \end{bmatrix} = \begin{bmatrix} H_1(\mathbf{X}) \\ H_2(\mathbf{X}) \end{bmatrix} + \begin{bmatrix} k_{1v} z_1 & k_{1v} z_2 \\ -k_{2v} z_2 & k_{2v} z_1 \end{bmatrix} \times \begin{bmatrix} v_{qs1-ref}^{e} \\ v_{ds1-ref}^{e} \end{bmatrix} = \mathbf{H_{12}}(\mathbf{X}) + \mathbf{D_{12}} \mathbf{U_{12}} \tag{27}$$

with

$$\mathbf{H_{12}}(\mathbf{X}) = \begin{bmatrix} k_{1v} E_1(\mathbf{X}) + \dot{v}_{qs2}^{e} - k_{1v} v_{qs2-ref}^{e} \\ k_{2v} E_2(\mathbf{X}) + \dot{v}_{ds2}^{e} - k_{2v} v_{ds2-ref}^{e} \end{bmatrix} \tag{28}$$

From Equs. (26) and (27), the equivalent SMC control action is obtained as

$$\mathbf{U_{ec}} = \begin{bmatrix} u_{ec1} \\ u_{ec2} \end{bmatrix} = -\mathbf{D_{12}}^{-1} \begin{bmatrix} H_1(\mathbf{X}) \\ H_2(\mathbf{X}) \end{bmatrix} \tag{29}$$

where $\boldsymbol{U}_{ec}$ is the vector of the two-axis reference voltages of the STATCOM. The control law described in Equ. (29) is changed to the following equation to guarantee the sliding mode reaching phase [25].

$$\begin{aligned} \mathbf{U_{12}} &= -\mathbf{D_{12}^{-1}} \left\{ \begin{bmatrix} H_1(\mathbf{X}) \\ H_2(\mathbf{X}) \end{bmatrix} + \begin{bmatrix} K_1 & 0 \\ 0 & K_2 \end{bmatrix} \begin{bmatrix} \text{sat}(S_1) \\ \text{sat}(S_2) \end{bmatrix} \right\} \\ &= -\mathbf{D_{12}^{-1}} [\mathbf{H_{12}}(\mathbf{X}) + \mathbf{K_{12}}\, \text{sat}(\mathbf{S_{12}})] \end{aligned} \tag{30}$$

with

$$\text{sat}\left(\frac{S_i}{\lambda_i}\right) = \begin{cases} 1 & S_i > \lambda_i \\ S_i / \lambda_i & |S_i| \le \lambda_i \\ -1 & S_i < -\lambda_i \end{cases} \tag{31}$$

where K_1 and K_2 are the positive control gains and λ_i is the saturation bandwidth of the sliding mode. The following Lyapunov function is nominated:

$$V_1 = \frac{1}{2} \mathbf{S_{12}^T S_{12}} = \frac{1}{2} S_1^2 + \frac{1}{2} S_2^2 \ge 0 \tag{32}$$

Taking the derivative of Eq. (32) yields

$$\dot{V}_1 = \frac{1}{2} (\dot{\mathbf{S}}_{\mathbf{12}}^{\mathbf{T}}) \mathbf{S_{12}} + \frac{1}{2} \mathbf{S_{12}^T} (\dot{\mathbf{S}}_{\mathbf{12}}) = S_1 \dot{S}_1 + S_2 \dot{S}_2 \tag{33}$$

By combining Equs. (27), (30), and (33), $\dot{V}_1$ is reduced to

$$\begin{aligned} \dot{V}_1 &= \mathbf{S_{12}^T} \dot{\mathbf{S}}_{\mathbf{12}} = -\mathbf{S_{12}^T K_{12}}\, \text{sat}(\mathbf{S_{12}}) \\ &= -K_1 S_1\, \text{sat}(S_1) - K_2 S_2\, \text{sat}(S_2) \le 0 \end{aligned} \tag{34}$$

Equ. (34) shows that $\dot{V}_1$ is a negative definite function; hence, the designed SMC is asymptotically stable.

A separate SMC for rotor speed control is designed such that no active power exchange takes place between the EW and the STATCOM. The following error signal is introduced:

$$e_{ps1} = P_{s1} - P_{s1-ref} = P_{s1} \tag{35}$$

with

$$P_{s1-ref} = 0 \quad , \quad P_{s1} = \frac{3}{2} (v_{ds1}^{e} i_{ds1}^{e} + v_{qs1}^{e} i_{qs1}^{e}) \tag{36}$$

where P_{s1} is the active power exchanged between the EW and the STATCOM and $P_{s1\text{-}ref}$ is its zero reference value. A switching surface is chosen as

$$S_3 = e_{ps1} + k_{1p} \int e_{ps1}\, dt \tag{37}$$

where K_{1p} is the positive constant of the SMC. Referring to [25], when the system states reach the sliding manifold and slide along the surface,

$$S_3 = \dot{S}_3 = 0 \tag{38}$$

Taking the derivative of Equ. (37) and replacing for P_{s1} and $\dot{P}_{s1}$ from Equ. (36) yields

$$\dot{S}_3 = \dot{P}_{s1} + k_{1p} P_{s1} = H_3(\mathbf{X}) + D_3(\mathbf{X})\, \omega_{r-ref} \tag{39}$$

The H_3 and D_3 functions are defined in Appendix B. As a result, the equivalent of the SMC control action is obtained by using Equs. (38) and (39).

$$\omega_{r-ref}^{ec} = -H_3(\mathbf{X}) / D_3(\mathbf{X}) \tag{40}$$

By utilizing Equ. (40), the following equivalent control law guarantees the sliding mode reaching phase [25]:

$$\omega_{r-ref} = -[H_3(\mathbf{X}) + k_{2p}\, \text{sat}(S_3)] / D_3(\mathbf{X}) \tag{41}$$

where k_{2p} is the positive control gain of the SMC.

The following Lyapunov function is nominated:

$$V_2 = \frac{1}{2} S_3^2 \ge 0 \tag{42}$$

Taking the derivative of Equ. (42) yields

$$\dot{V}_2 = S_3 \dot{S}_3 \tag{43}$$

Combining Equs. (39), (41), and (43) results in

$$\begin{aligned} \dot{S}_3 &= -k_{2p}\, \text{sat}(S_3) \\ \dot{V}_2 &= -k_{2p} S_3\, \text{sat}(S_3) \le 0 \end{aligned} \tag{44}$$

Equ. (44) shows that $\dot{V}_2$ is a negative definite function; hence, the designed SMC is asymptotically stable.

IV. Simulation Results

By using a 1.8 kW six-phase CRIG, whose parameters are given in Table I, along with a regulated speed wind turbine based on a pitch angle controller and following the theory mentioned in the previous sections, a C++ computer program is developed to solve the nonlinear differential equations of the generator. The static fourth-order Runge–Kutta method is used to solve these equations.

Consider a three-phase static *(R* = 90 Ω, *L* = 0.175 H*)*

TABLE I
GENERATOR PARAMETERS

Number of pole pairs	*Pole*	1
Frequency	f_n	50 Hz
Power	P_n	1.8 kW
Stator line voltages	V_L	380 V
Stator line currents	I_L	3.5 A
Stator EW resistance	R_{s1}	2.4 Ω
Stator PW resistance	R_{s2}	2.4 Ω
Rotor resistance	R_r	4.1 Ω
Stator EW leakage inductance	L_{ls1}	11 mH
Stator PW leakage inductance	L_{ls2}	11 mH
Rotor leakage inductance	L_{lr}	11 mH
Magnetization inductance	L_m	374 mH
EW and PW spatial phase difference	α	30°
Inertia momentum	J	0.038 Kgm^2

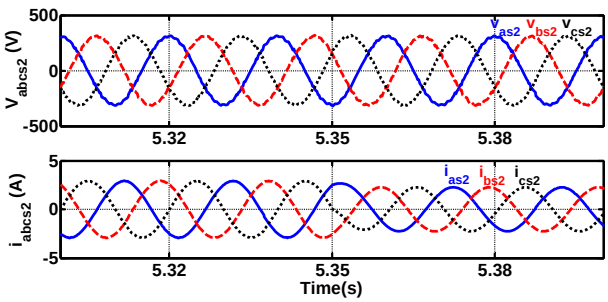

Fig. 4. Three-phase voltages and currents of the generator output.

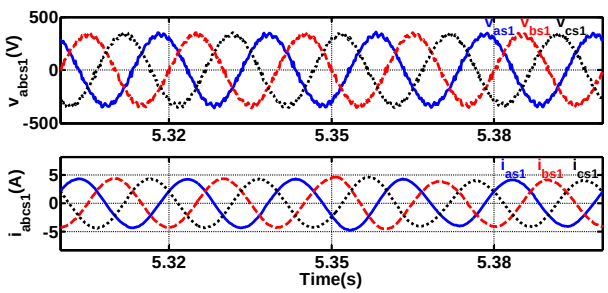

Fig. 5. Excitation voltage and current of the generator.

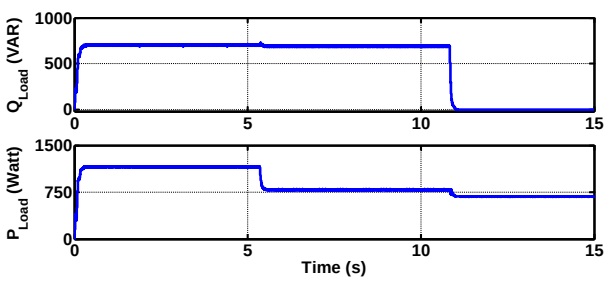

Fig. 6. Active and reactive powers of the load.

balanced load connected to the generator output terminals at t = 0 s. This three-phase static balanced load is stepped change to (R = 103 Ω, L = 0.286 H) at t = 5.35 s and to (R = 210 Ω, L = 0 H) at t = 10.83 s. The simulation results obtained from these tests are shown in Figs. 4-9. The three-phase voltage and current waveforms of the load are shown in Fig. 4. The three-phase voltage and current waveforms of the EW input are presented in Fig. 5. The three-phase STATCOM is connected to the EW via an L-C low-pass filter with a cut-off frequency of 1 kHz. This filter is capable of filtering out the high-order harmonics of the STATCOM. As a result, an approximate sinusoidal rotating flux density wave is generated.

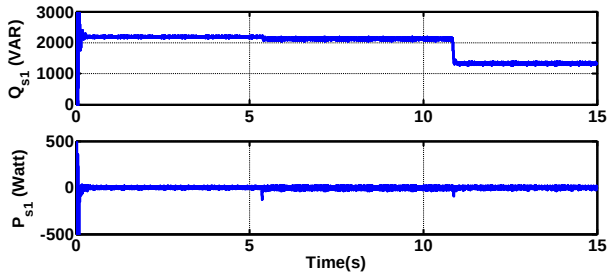

Fig. 7. EW input powers.

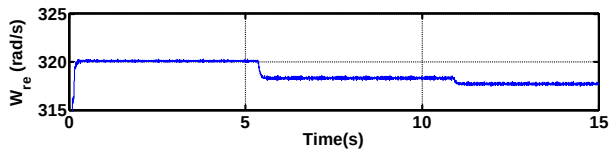

Fig. 8. Rotor angular speed in electrical rad/s.

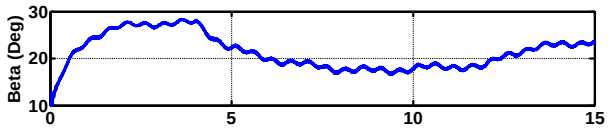

(a) Pitch angle of blades.

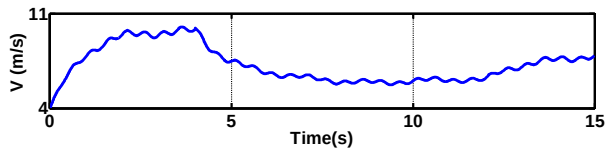

(b) Wind speed.

Fig. 9. Wind turbine parameters.

Fig. 6 shows the active and reactive power waveforms of the load. Fig. 7 shows the waveforms of the active and reactive powers of the EW input; as expected, no active power is exchanged between the EW and the STATCOM. Fig. 8 illustrates the rotor electrical angular speed variation. Fig. 9 demonstrates the wind linear speed and wind turbine pitch angular variations.

V. EXPERIMENTAL RESULTS

A PC-based setup is designed and implemented for the closed-loop control of the IGS shown in Fig. 1. In this control system, a 1.8 kW six-phase CRIM, whose parameters are given in Table I, and a 2.2 kW dc motor are employed. The experimental setup shown in Figs. 10–11 consists of the following sections.

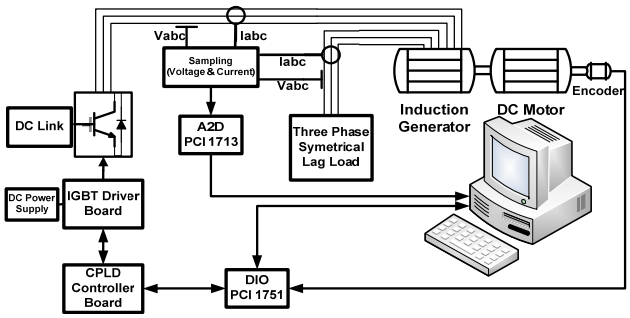

Fig. 10. Block diagram of the experimental setup.

A three-phase voltage source inverter is equipped with an isolation board, voltage and current sampling boards, a 48-bit Advantech digital input–output card, a 32-channel Advantech A/D converter card, a CPLD board, and a PC for data processing. An Altera EPM240T100 CPLD is employed to obtain SV-PWM inverter switching patterns with a 5 kHz switching frequency. The CPLD board is set to communicate with the PC via a digital Advantech PCI-1751 I/O board. The CPLD used in the experimental setup is realized as follows: a switching pattern is generated with the SV-PWM technique for IGBT switches; a useful dead time is provided in the so-called switching patterns of the power switches; a synchronizing signal is generated for the data transmission between the PC and the hardware; the inverter is shut down in case of emergency conditions, such as overcurrents or PC hanging states. The designed SV-PWM inverter is implemented by using six single switches of STGW30NC120HD. HCPL316J IC is used to design a fast and intelligent IGBT driver that guarantees a reliable isolation between the high voltage and control boards. The dc-link voltage, along with the voltages and currents of the two stator windings, is measured with Hall-type LEM sensors of LA55P and LV20P. All the measured electrical signals are filtered and then converted into digital signals using an Advantech PCI 1713-U A/D card. The actual rotor position is detected with an absolute encoder with 1024 pulses/rev. In addition, an L-C low-pass filter with a cut-off frequency of 1 kHz is employed to filter out the high-order harmonics of the STATCOM. As a result, a nearly sinusoidal rotating flux density wave is obtained.

An existing separately excited dc motor equipped with a closed-loop speed control system is used as the generator prime mover. The three-phase symmetrical load of the generator is obtained by combining a small three-phase induction motor in parallel with several 40 W incandescent lamps at $t = 0$ s. At $t =$ 5.35 s, approximately 35% of the lamps are turned off. The three-phase induction motor is finally switched off at $t = 10.83$ s. The experimental results obtained from these tests are shown in Figs. 12-16. As revealed by the comparison of the simulation and experimental results, extra high-frequency oscillations exist in the wave shapes of the experimental results because of the existence of noises in the laboratory. These noises are

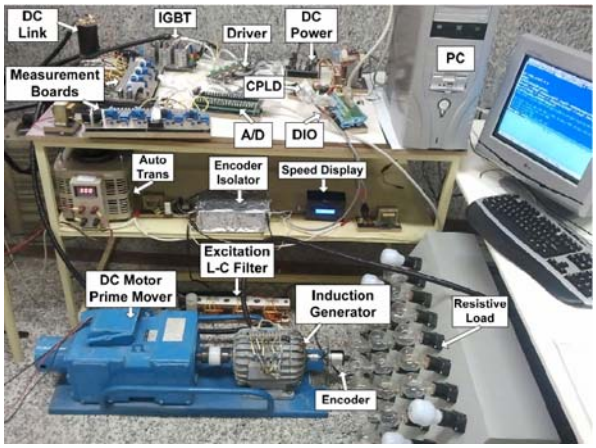

Fig. 11. Experimental setup.

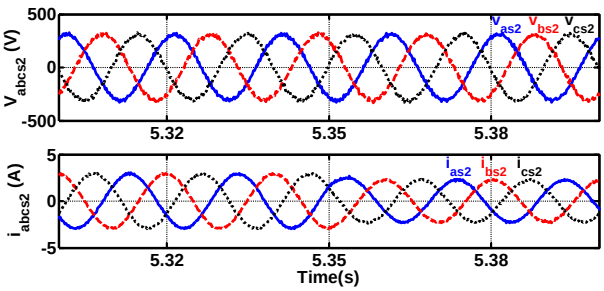

Fig. 12. Output voltage and current of the generator.

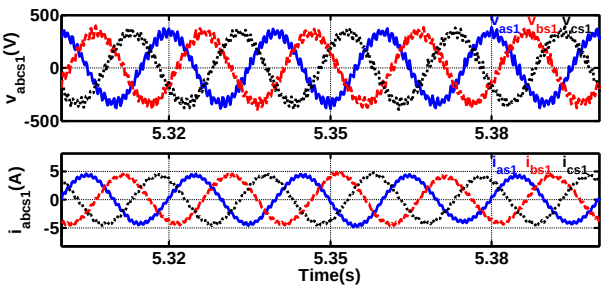

Fig. 13. Excitation voltage and current of the generator.

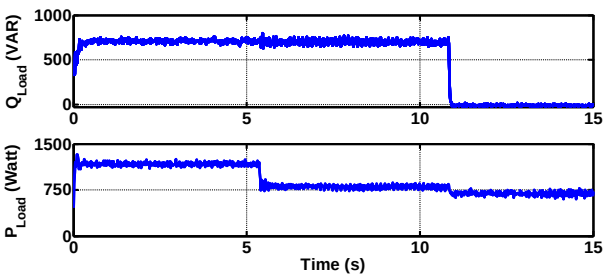

Fig. 14. Active and reactive powers of the load.

mainly generated by the PWM inverter switching process or environmental electro-magnetic sources.

For a desired load power demand, the employed prime mover must regulate the rotor speed corresponding to the reference value obtained by the second SMC. Therefore, it does not matter which type of mechanical prime mover with

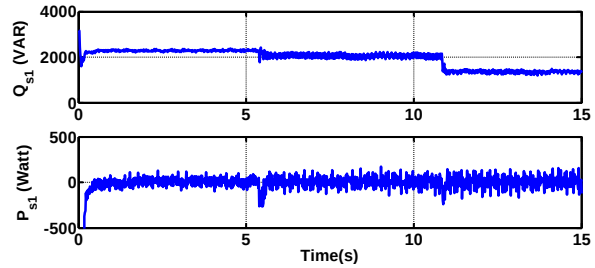

Fig. 15. EW input powers.

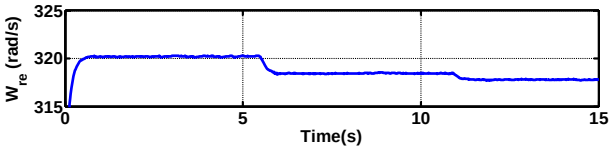

Fig. 16. Rotor angular speed in electrical rad/s.

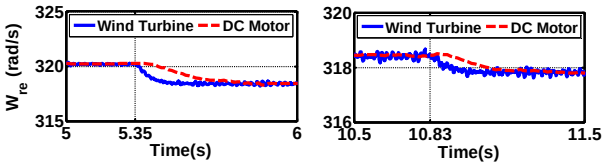

Fig. 17. Dynamic responses of the wind turbine and dc motor.

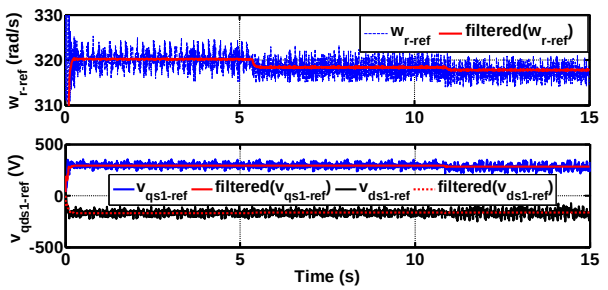

Fig. 18. Reducing SMC chattering with a software low-pass filter.

adjustable speed is used. Although different prime movers are utilized for the simulation and experimental results, the two sets of results show excellent agreement. The slight difference between these results during generator load changing, especially with regard to the active power of the EW input (Figs. 7 and 15), is due to the faster dynamic response of the wind turbine pitch control in comparison with that of the dc motor speed control (Fig. 17). The fast dynamic response of a generator prime mover equates to low active power exchanged between the generator and the STATCOM. As the dynamic response of the dc motor control system is slower than that of the wind turbine, higher jump points can be observed in Fig. 15 in comparison with those in Fig. 7 during load step changing.

As a result of the use of a narrow bandwidth sliding mode saturation layer and software low-pass filters, a low sliding mode chattering is achieved, as shown in Fig. 18.

V. Conclusion

A new stand-alone three-phase IGS with constant frequency and regulated output voltage is proposed. This IGS employs a six-phase cage induction machine with two separate and balanced three-phase stator windings. The first stator winding set connected to an SV-PWM STATCOM is used to excite the machine, and the second stator winding set is directly connected to a desired three-phase load. The load voltage is regulated by an SMC to enable the controller to determine the reference voltages of the STATCOM. The fundamental reference frequency of the STATCOM is chosen to be equal to the desired output frequency of the generator. A second SMC is developed and used to regulate the zero active power exchanged between the STATCOM and the stator excitation winding. Upon the selection of a constant frequency and for a desired generator load, the second SMC identifies the rotor reference rotating speed. This IGS is implemented theoretically via a computer simulation and practically via an experimental setup designed and built for this purpose. The experimental results are obtained with a dc motor as the generator prime mover, whereas the simulation results are obtained with a pitch angle-controlled wind turbine. Although different prime movers are used, the two sets of results show excellent agreement. Simulation and experimental results confirm the feasibility and effectiveness of the proposed IGS.

Appendix

A. IGS Model Functions and Coefficients

$$f_1 = a_{12}v^e_{qs2} + a_{13}v^e_{ds2} + a_{14}i^e_{qs1} + a_{15}i^e_{ds1} + a_{16}\lambda^e_{qs1} + a_{17}\lambda^e_{ds1} + a_{18}i^e_{qs2} + a_{19}i^e_{ds2}$$

$$f_2 = -a_{13}v^e_{qs2} + a_{12}v^e_{ds2} - a_{15}i^e_{qs1} + a_{14}i^e_{ds1} - a_{17}\lambda^e_{qs1} + a_{16}\lambda^e_{ds1} - a_{19}i^e_{qs2} + a_{18}i^e_{ds2}$$

$$f_3 = -R_{s1}i^e_{qs1} - \omega_e\lambda^e_{ds1} \quad , \quad f_4 = -R_{s1}i^e_{ds1} + \omega_e\lambda^e_{qs1}$$

$$f_5 = a_{23}v^e_{qs2} + a_{24}i^e_{qs1} + a_{25}i^e_{ds1} + a_{26}\lambda^e_{qs1} + a_{27}\lambda^e_{ds1} + a_{28}i^e_{qs2} + a_{29}i^e_{ds2}$$

$$f_6 = a_{23}v^e_{ds2} - a_{25}i^e_{qs1} + a_{24}i^e_{ds1} - a_{27}\lambda^e_{qs1} + a_{26}\lambda^e_{ds1} - a_{29}i^e_{qs2} + a_{28}i^e_{ds2}$$

$$f_7 = [\frac{-3}{2}(\lambda^e_{ds2}i^e_{qs2} - \lambda^e_{qs2}i^e_{ds2}) - B\omega_r]/J$$

$$a_{11} = (L_{lr}L_m + L_{ls2}L_r)/[L_m(L_{ls1}L_{lr} - G_3L_{ls2})]$$

$$a_{12} = -L_{lr}\cos\alpha/(G_3L_{ls2} - L_{ls1}L_{lr})$$

$$a_{13} = L_{lr}\sin\alpha/(G_3L_{ls2} - L_{ls1}L_{lr})$$

$$a_{14} = [R_{s1}L_{lr}L_m + L_{ls2}(R_{s1}L_r + R_rL_{s1})]/L_m(G_3L_{ls2} - L_{ls1}L_{lr})$$

$$a_{15} = [\omega_eL_{ls1}L_{lr} - G_3(\omega_e - \omega_r)L_{ls2}]/(G_3L_{ls2} - L_{ls1}L_{lr})$$

$$a_{16} = -R_rL_{ls2}/[L_m(G_3L_{ls2} - L_{ls1}L_{lr})]$$

$$a_{17} = \omega_rL_rL_{ls2}/[L_m(G_3L_{ls2} - L_{ls1}L_{lr})]$$

$$a_{18} = [(R_r\cos\alpha - (\omega_e - \omega_r)L_{lr}\sin\alpha)L_{ls2} - (R_{s2}\cos\alpha - \omega_eL_{ls2}\sin\alpha)L_{lr}]/(G_3L_{ls2} - L_{ls1}L_{lr})$$

$$a_{19}=[(R_r\sin\alpha+(\omega_e-\omega_r)L_{lr}\cos\alpha)L_{ls2}-(R_{s2}\sin\alpha+\omega_e L_{ls2}\cos\alpha)L_{lr}]/(G_3L_{ls2}-L_{ls1}L_{lr})$$

$$a_{21}=-\cos\alpha(G_3L_m+L_{ls1}L_r)/[L_m(G_3L_{ls2}-L_{ls1}L_{lr})]$$

$$a_{22}=\sin\alpha[G_3L_m+L_{ls1}L_r]/[L_m(G_3L_{ls2}-L_{ls1}L_{lr})]$$

$$a_{23}=G_3/(G_3L_{ls2}-L_{ls1}L_{lr})$$

$$a_{24}=[R_{s1}L_rL_{ls1}\cos\alpha-(\omega_e-\omega_r)G_3L_{ls1}L_m\sin\alpha+R_rL_{s1}L_{ls1}\cos\alpha+(R_{s1}\cos\alpha+\omega_eL_{ls1}\sin\alpha)\times L_mG_3]/[L_m(G_3L_{ls2}-L_{ls1}L_{lr})]$$

$$a_{25}=-[(R_{s1}L_{ls1}L_r\sin\alpha+(\omega_e-\omega_r)G_3L_{ls1}L_m\times\times\cos\alpha+R_rL_{ls1}L_{s1}\sin\alpha+(R_{s1}\sin\alpha-\omega_eL_{ls1}\cos\alpha)\times L_mG_3]/[L_m(G_3L_{ls2}-L_{ls1}L_{lr})]$$

$$a_{26}=L_{ls1}[-R_r\cos\alpha+\omega_rL_r\sin\alpha]/[L_m(G_3L_{ls2}-L_{ls1}L_{lr})]$$

$$a_{27}=L_{ls1}[R_r\sin\alpha+\omega_rL_r\cos\alpha]/[L_m(G_3L_{ls2}-L_{ls1}L_{lr})]$$

$$a_{28}=(R_rL_{ls1}-G_3R_{s2})/(G_3L_{ls2}-L_{ls1}L_{lr})$$

$$a_{29}=[(\omega_e-\omega_r)L_{ls1}L_{lr}-G_3\omega_eL_{ls2}]/(G_3L_{ls2}-L_{ls1}L_{lr})$$

B. SMC Functions and Coefficients

$$G_3=(L_m^2-L_{s1}L_r)/L_m$$

$$G_4=1+a_{12}L_{ls1}\cos\alpha-a_{23}L_{ls2}+a_{13}L_{ls1}\sin\alpha$$

$$b_1=(a_{21}L_{ls2}+\cos\alpha-a_{11}L_{ls1}\cos\alpha)/G_4$$

$$b_2=(a_{22}L_{ls2}-\sin\alpha+a_{11}L_{ls1}\sin\alpha)/G_4$$

$$b_3=(-a_{14}L_{ls1}\cos\alpha+a_{24}L_{ls2}-R_{s1}\cos\alpha-a_{15}L_{ls1}\sin\alpha-\omega L_{ls1}\sin\alpha)/G_4$$

$$b_4=(-a_{15}L_{ls1}\cos\alpha+a_{25}L_{ls2}+R_{s1}\sin\alpha+a_{14}L_{ls1}\sin\alpha-\omega L_{ls1}\cos\alpha)/G_4$$

$$b_5=(-a_{18}L_{ls1}\cos\alpha+a_{28}L_{ls2}+R_{s2}-a_{19}L_{ls1}\sin\alpha)/G_4$$

$$b_6=(-a_{19}L_{ls1}\cos\alpha+a_{29}L_{ls2}+a_{18}L_{ls1}\sin\alpha+\omega L_{ls2})/G_4$$

$$b_7=(-a_{16}L_{ls1}\cos\alpha+a_{26}L_{ls2}-a_{17}L_{ls1}\sin\alpha)/G_4$$

$$b_8=(-a_{17}L_{ls1}\cos\alpha+a_{27}L_{ls2}+a_{16}L_{ls1}\sin\alpha)/G_4$$

$$b_9=(a_{13}L_{ls1}\cos\alpha-a_{12}L_{ls1}\sin\alpha)/G_4$$

$$z_1=(b_1+b_2b_9)/(1+b_9^2)\quad,\quad z_2=(b_2-b_1b_9)/(1+b_9^2)$$

$$E_1=((b_3+b_9b_4)i^e_{qs1}+(b_4-b_9b_3)i^e_{ds1}+(b_5+b_9b_6)i^e_{qs2}+(b_6-b_9b_5)i^e_{ds2}+(b_9b_8+b_7)\lambda^e_{qs1}+(b_8-b_9b_7)\lambda^e_{ds1})/(1+b_9^2)$$

$$E_2=((b_9b_3-b_4)i^e_{qs1}+(b_3+b_9b_4)i^e_{ds1}+(b_9b_5-b_6)i^e_{qs2}+(b_5+b_9b_6)i^e_{ds2}+(b_9b_7-b_8)\lambda^e_{qs1}+(b_7+b_9b_8)\lambda^e_{ds1})/(1+b_9^2)$$

$$D_3=\frac{3}{2}[(v^e_{qs1}i^e_{qs2}+v^e_{ds1}i^e_{ds2})L_{lr}L_{ls2}L_m\sin\alpha-(v^e_{qs1}i^e_{ds2}-v^e_{ds1}i^e_{qs2})L_{lr}L_{ls2}L_m\cos\alpha+G_3L_{ls2}L_m(v^e_{qs1}i^e_{ds1}-v^e_{ds1}i^e_{qs1})+(v^e_{qs1}\lambda^e_{ds1}-v^e_{ds1}\lambda^e_{qs1})L_rL_{ls2}]/[L_m(G_3L_{ls2}-L_{ls1}L_{lr})]$$

$$H_3=\frac{3}{2}[v^e_{ds1}(a_{11}v^e_{ds1}-a_{13}v^e_{qs2}+a_{12}v^e_{ds2}-a'_{15}i^e_{qs1}+a_{14}i^e_{ds1}+a_{16}\lambda^e_{ds1}-a'_{19}i^e_{qs2}+a'_{18}i^e_{ds2})+v^e_{qs1}(a_{11}v^e_{qs1}+a_{12}v^e_{qs2}+a_{13}v^e_{ds2}+a_{14}i^e_{qs1}+a'_{15}i^e_{ds1}+a_{16}\lambda^e_{qs1}+a'_{18}i^e_{qs2}+a'_{19}i^e_{ds2})+(i^e_{ds1}\dot{v}^e_{ds1}+i^e_{qs1}\dot{v}^e_{qs1})+k_{1p}(v^e_{ds1}i^e_{ds1}+v^e_{qs1}i^e_{qs1})]$$

where the a'_{ij} coefficients are obtained by dropping the ω_r terms in the a_{ij} coefficients.

REFERENCES

[1] K. Singh, "Modeling and experimental analysis of a self-excited six-phase induction generator for stand-alone renewable energy generation," *Renewable Energy,* Vol. 33, No. 7, pp. 1605-1621, Jul. 2008.

[2] D. Wang, W. Ma, F. Xiao, B. Zhang, D. Liu, and A. Hu, "A novel stand- alone dual stator winding induction generator with static excitation regulation," *IEEE Trans. Energy Convers.*, Vol. 20, No. 4, pp. 826-835, Dec. 2006.

[3] B. Singh, S. S. Murthy, and S. Gupta, "A solid state controller for self-excited induction generator for voltage regulation, harmonic compensation and load balancing," *Journal of Power Electronics,* Vol. 5, No. 2, pp. 109-119, Apr. 2005.

[4] T. F. Chan and L. L. Lai, "A novel excitation scheme for a stand-alone three-phase induction generator supplying single-phase loads," *IEEE Trans. Energy Convers.,* Vol. 19, No. 1, pp. 136-143, Mar. 2004.

[5] S. S. Murthy, B. Singh, S. Gupta, and B. M. Gulati, "General steady-state analysis of three-phase self-excited induction generator feeding three-phase unbalanced load/single-phase load for stand-alone applications," *IEE Proc. Gener. Transm. Distrib.,* Vol. 150, No. 1, pp. 49-55, Jan. 2003.

[6] S. K. Jain, J. D. Sharma, and S. P. Singh, "Transient performance of three-phase self-excited induction generator during balanced and unbalanced faults," *IEE Proc. Gener .Transm. Distrib.,* Vol. 149, No. 1, pp. 50-57, Jan. 2002.

[7] T. Ahmed, O. Noro, E. Hiraki, and M. Nakaoka, "Terminal voltage regulation characteristics by static var compensator for a three-phase self-excited induction generator," *IEEE Trans. Ind. Appl.,* Vol. 40, No. 4, pp. 978-988, Jul./Aug. 2004.

[8] S. Hazra and P. Sensarma, "Vector approach for self-excitation and control of induction machine in stand-alone wind power generation," *IET Renewable Power Generation,* Vol. 5, No. 5, pp. 397-405, 2011.

[9] B. R. Karthikeya and R. J. Schütt, "Overview of Wind Park Control Strategies," *IEEE Trans. Sustain. Energy,* Vol. 5, No. 2, pp. 416-422, Apr. 2014.

[10] V. Phan, H. Leey, and T. Chun, "An improved control strategy using a PI-resonant controller for an unbalanced stand-alone doubly-fed induction generator," *Journal of Power Electronics,* Vol. 10, No. 2, pp. 194-202, Mar. 2010.

[11] P. B. Reddy, K. K. Huh, and A. M. El-Refaie, "Generalized approach of stator shifting in interior permanent-magnet machines equipped with fractional-slot concentrated windings," *IEEE Trans. Ind. Electron.,* Vol. 61, No. 9, pp. 5035-5046, Sep. 2014.

[12] H. S. Che, E. Levi, M. Jones, M. J. Duran, W. Hew, and N.

A. Rahim, "Operation of a six-phase induction machine using series-connected machine-side converters," *IEEE Trans. Ind. Electron.,* Vol. 61, No. 1, pp. 164-176, Jan. 2014.
[13] G. K. Singh, K. B. Yadav, and R. P. Saini, "Capacitive self-excitation in a six-phase induction generator for small hydro power – An experimental investigation," in *Proc. PEDES,* pp. 1-6, 2006.
[14] Y. Li, Y. Hu, W. Huang, L. Liu, and Y. Zhang, "The capacity optimization for the static excitation controller of the dual-stator-winding induction generator operating in a wide speed range," *IEEE Trans. Ind. Electron.,* Vol. 56, No. 2, pp. 530-541, Feb. 2009.
[15] S. Shao, T. Long, E. abdi, and R. A. McMahon, "Dynamic control of the brushless doubly fed induction generator under unbalanced operation," *IEEE Trans. Ind. Electron.,* Vol. 60, No. 6, pp. 2465-2476, Jun. 2013.
[16] F. Bu, Y. Hu, W. Huang, S. Zhuang, and K. Shi, "Control strategy and dynamic performance of dual stator-winding induction generator variable frequency AC generating system with inductive and capacitive loads," *IEEE Trans. Power Electron.,* Vol. 29, No. 4, pp. 1681-1692, Apr.2014.
[17] F. Bu, W. Huang, Y. Hu, J. Shi, and K. Shi, "A stand-alone dual stator winding induction generator variable frequency AC power system," *IEEE Trans. Power Electron.*, Vol. 27, No. 1, pp. 10-13, Jan. 2012.
[18] F. Bu, Y. Hu, W. Huang, and S. Zhuang, "Parameter design and static performance of dual stator-winding induction generator variable frequency AC generating system with inductive and capacitive loads," *IEEE Trans. Ind. Electron.,* Vol. 61, No. 8, pp. 3902-3914, Aug. 2014.
[19] O. Ojo, O. Omozusi, A. Ginart, and B. Gonoh, "The operation of a stand-alone single-phase induction generator using a single-phase pulse-width modulated inverter with a battery supply," *IEEE Trans. Energy Convers.*, Vol. 14, No. 3, pp. 526-531, Sep. 1999.
[20] J. Soltani and N. R. Abjadi, "A novel stand-alone single phase induction generator using a 3-phase machine and a single phase PWM inverter," in *Proc. EPE PEMC*., 2002.
[21] J. Soltani, Y. Hassani, and N. R. Abjadi, "A novel isolated three-phase induction generator with constant frequency and adjustable output voltage using a three-phase STATCOM," in *Proc. ICCESSE,* 2012.
[22] P. Vas, *Electrical Machines and Drives: A Space-Vector Theory Approach*, pp. 87-134, Clarendon Press, 1992.
[23] Z. Zhang, Q. Zhou, and A. Kusiak, "Optimization of wind power and its variability with a computational intelligence approach," *IEEE Trans. Sustain. Energy,* Vol. 5, No. 1, pp. 228-236, Jan. 2014.
[24] M. J. Hossain, H. R. Pota, V. A. Ugrinovski, and R. A. Ramos, "Simultaneous STATCOM and pitch angle control for improved LVRT capability of fixed-speed wind turbines," *IEEE Trans. Sustain. Energy,* Vol. 1, No. 3, pp. 142–151, Oct. 2010.
[25] J. J. E. Slotine and W. Li, *Applied Nonlinear Control*, pp. 277-300, Englewood Cliffs, NJ: Prentice Hall, 1991.

Mohammadreza Moradian was born in Isfahan, Iran, in 1975. He received his B.Sc. and M.Sc. degrees in Electrical Engineering from the Isfahan University of Technology, Isfahan, Iran, in 1998 and 2000, respectively. He is currently working toward a Ph.D. degree in Electrical Engineering at the Islamic Azad University, Science and Research Branch, Tehran, Iran. He has been a faculty member of the Electrical Engineering Department of Islamic Azad University, Najafabad Branch, since 2001. His research interests include electrical machines, power electronics, and renewable energy generation systems.

Jafar Soltani graduated from Tabriz University, Tabriz, Iran, in 1974 and received his M.S. and Ph.D. degrees from the University of Manchester Institute of Science and Technology, Manchester (U.M.I.S.T), U.K., in 1983 and 1987, respectively. He is currently a Professor in the Islamic Azad University, Khomeini-Shahr Branch, Department of Electrical & Computer Engineering, Isfahan, Iran. He is also an Emeritus Professor in the Faculty of Electrical & Computer Engineering, Isfahan University of Technology, Isfahan, Iran. His main areas of research include electrical machines and drives, power electronics, and power system control. He has published many international journal and conference papers and is a holder of a U.K. patent.